Observation of laser-induced field-free permanent planar alignment of molecules

Md. Z. Hoque, M. Lapert, E. Hertz, F. Billard, Dominique Sugny, B. Lavorel, O. Faucher

Observation of laser-induced field-free permanent planar alignment of molecules

Md. Z. Hoque, M. Lapert, E. Hertz, F. Billard, D. Sugny,* B. Lavorel, and O. Faucher†
Laboratoire Interdisciplinaire Carnot de Bourgogne (ICB), UMR 5209 CNRS-Université de Bourgogne, 9 Av. A. Savary, BP 47 870, F-21078 DIJON Cedex, FRANCE
(Dated: November 15, 2011)

Permanent planar alignment of gas-phase linear molecules is achieved by a pair of delayed perpendicularly polarized short laser pulses. The experiment is performed in a supersonic jet ensuring a relatively high number density of molecules with moderately low rotational temperature. The effect is optically probed on a femtosecond time scale by the use of a third short pulse, enabling a time-resolved birefringence detection performed successively in two perpendicular planes of the laboratory frame. The technique allows for an unambiguous estimation of the molecular planar delocalization produced within the polarization plane of the pulse pair after the turn-off of the field. The measurements are supported by numerical simulations which lead to the quantification of the observed effect and provide more physical insights into the phenomenon.

PACS numbers: 37.10.Vz, 42.50.Hz, 42.50.Md

I. INTRODUCTION

The space handling of molecules is a fascinating topic that has received during these last years a growing attention. In particular, molecular alignment induced by a laser field was shown to be practically useful in various fields extending to high-harmonic generation and attophysics [1, 2], molecular tomography [3, 4], molecular-frame photoelectron angular distribution [5–7], ultrafast all-optical switching of electrical junctions [8], laser filamentation [9], ultrafast optical imaging [10, 11], generation of terahertz radiation [12, 13], and so forth. Although the mechanisms at play in molecular alignment are now well understood, as documented in both experimental [14, 15] and theoretical [16] works, valuable strategies that aim at optimizing angular focusing [17, 18] or at preparing angular distributions designed for specific applications [19] remain a current challenge.

Recently, the ultrafast orientation of the angular momentum of a symmetric top molecule has been achieved using a sequence of two short laser pulses, properly delayed and polarized at 45° with respect to each other [20]. The field arrangement enables the production of an asymmetric distribution of the helicity quantum number M, defined as the projection of the total angular momentum $\vec{J}$ along the quantization axis, supporting the rotation of the molecules in one sense rather than in the other [21, 22]. At the same time, a strategy to produce a field-free permanent molecular planar alignment was proposed [23]. The two previous approaches mainly differ by the relative intensity, the delay, and more importantly, the mutual polarization between the two pulses. In the latter, the two pulses form an angle of 90° in order to optimize the confinement of the molecular axis in the polarization plane, which is performed to the detriment of the orientation of the angular momentum achieved in the former.

Permanent planar alignment is relevant for various applications including stereodynamics effects of elementary processes. For instance, it can play an important role on the adsorption of molecules on a surface [24, 25]. The scattering of molecules through electrostrictive forces [26] is also influenced by the rotation of the molecules [27]. Very recently, it has been shown that the deflection angles can be controlled by tilting the plane of rotation of the molecule prepared in a state of planar alignment [28].

II. METHODS

Hereby, we provide an experimental realization of permanent planar alignment by demonstrating the effect for a linear molecule. We consider two short laser pulses copropagating along the z axis and linearly polarized along two different coordinate axes of the laboratory frame, e.g. x and y, respectively. Both pulses, of same wavelength, are temporally delayed by $T_{\rm r}/2$, where $T_{\rm r}$ is the rotational period of the molecule. Each pulse individually produces a non-adiabatic alignment of the linear molecule along its respective polarization axis [14], featured by field-free revivals occurring at fractional times of the rotational period superimposed on a permanent alignment component. However, the collective action of the two pulses results on a transient alignment of the molecular axis that alternates between the two x and y directions during each revival. More importantly, it also leads to a quasi steady confinement of the molecular axis in the (xy) plane [23].

This permanent planar alignment can be understood in a first approach in terms of selection rules. The alignment proceeds from the non-resonant impulsive Raman excitation of the molecular polarizability resulting in a rotational wave packet produced in the ground vibronic state of the molecule. Considering first a single linearly polarized pulse, the electric-dipole-allowed Raman

*Electronic address: dominique.sugny@u-bourgogne.fr
†Electronic address: olivier.faucher@u-bourgogne.fr

transitions satisfy the selection rules $\Delta J = 0, \pm 2$ and $\Delta M = 0$. Starting from the initial condition $|J_0, M_0\rangle$, the $|J \gg J_0, M_0\rangle$ states are populated through stepwise excitation during the strong pulse interaction. The angular distribution of these unequally populated helicity states correspond to a confinement of the molecular axis along the quantization axis, i.e. the field direction, together with a delocalization of the total angular momentum in the equatorial plane. Considering now the sequence of cross-polarized pulses introduced above, the total field, in addition, leads to $\Delta M = \pm 2$ transitions, enabling the population of the $|J \gg J_0, |M| \gg |M_0|\rangle$ levels. These spatially anisotropic states, in particular those for which $M \simeq J$ and $M \simeq -J$, represent respectively the molecules with an angular momentum J pointing along the two opposite directions of the quantization axis z. For the pulse delay $T_r/2$, the superposition of the free-evolving states populated during the pulse interactions leads to a quasi-symmetric distribution in M, with an angular momentum aligned along the z axis, and to a confinement of the molecular axis in the plane of polarization spanned by the two field vectors [23].

III. RESULTS AND DISCUSSION

A. Experiment

In order to track the free evolution of the system prepared by the bi-pulse, we optically probe the molecules with a third delayed pulse [29]. The experiment is performed on the CO_2 molecule. For a better efficiency of the process, the molecules are rotationally cooled down to a temperature of the order of 100 K in a supersonic expansion of a continuous jet. The number density estimated at the interaction region is close to 10^{19}cm^{-3}. For this study, the relevant observable is $\langle\cos^2\theta_z\rangle$, with $\langle\cdot\rangle$ indicating the quantum expectation value and θ_z the angle of the molecular axis with respect to the propagation z axis. A planar alignment in the polarization (xy) plane is achieved when $\langle\cos^2\theta_z\rangle < 1/3$, whereas $\langle\cos^2\theta_z\rangle > 1/3$ reflects an alignment along the z axis, $1/3$ being the degree of alignment at thermal equilibrium. In principle, a cross-Kerr defocusing technique allows to reveal the value of $\langle\cos^2\theta_z\rangle$ from the spatial modification of the refractive index measured by a probe field polarized along the z axis [30, 31]. However, it has been shown that experiments performed with this technique at large peak intensity suffer from an additional signal produced by the free electrons due to the ionization of the gas sample [32]. For this reason, we have employed a time-resolved polarization technique immune to plasma effects, and particularly sensitive for probing molecular alignment of linear [33–36] and asymmetric top molecules [37]. It consists in measuring the transient birefringence experienced by a probe pulse linearly polarized at 45° with respect to a pair of space-fixed axes i, j. In heterodyne detection [38], the birefringence signal denoted as $\mathcal{S}_{ij}$ is proportional to

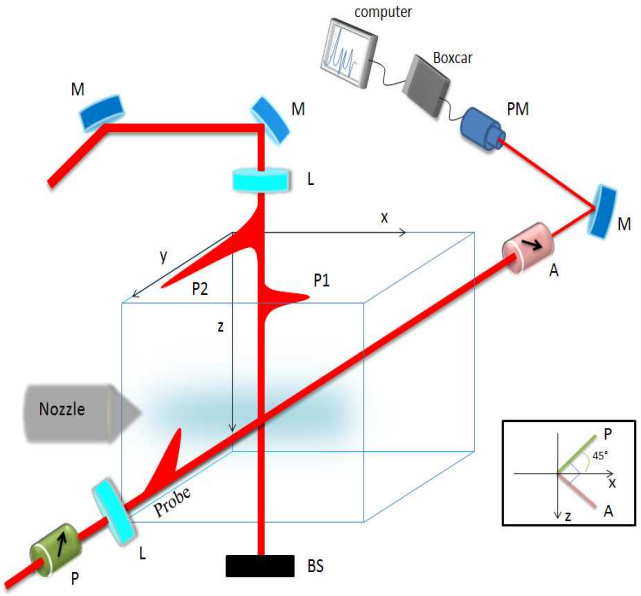

FIG. 1: (Color online) Schematic diagram depicting the arrangement of the probe and the two pulses P_1 and P_2 used to generate a planar alignment in the (xy) plane. M: Mirrors, L: Lens, P: Polarizer, A: Analyzer, BS: Beam stop, PM: Photomultiplier. The relative polarizations of the probe (P) and signal-field (A) are shown in the inset.

$n_i - n_j \simeq \frac{\varrho\Delta\alpha}{2\overline{n}\varepsilon_0}\left(\langle\cos^2\theta_i\rangle - \langle\cos^2\theta_j\rangle\right)$, where $n_{l=x,y,z}$ is the optical Kerr index produced along the l axis, ϱ the number density, $\overline{n} = 1/2(n_i + n_j)$, ε_0 the vacuum permittivity, and $\Delta\alpha = \alpha_\parallel - \alpha_\perp$ the polarizability anisotropy with $\alpha_\parallel$ and $\alpha_\perp$ being respectively the polarizability components parallel and perpendicular to the internuclear axis [37]. Using the geometric relation $\sum_l \langle\cos^2\theta_l\rangle = 1$ between the director cosines, any expectation value $\langle\cos^2\theta_i\rangle$ can be deduced from a combination of birefringence signals recorded between two distinct pairs of space-fixed axes. It is easy to show for instance that the value of interest $\langle\cos^2\theta_z\rangle$ can be obtained from a combination of $\mathcal{S}_{xz}$ and $\mathcal{S}_{yz}$.

Aligning and probing beams are produced by a chirped pulse amplified Ti:sapphire femtosecond laser. The system provides 100 fs-duration pulses at a repetition rate of 100 Hz, with a wavelength centered at 800 nm. At first, a series of measurements is conducted by setting the three pulses as depicted in Fig. 1. The aligning pulse P_1 (resp., P_2) of intensity I_1 (resp., I_2) propagates along the z axis with a field linearly polarized along the x (resp. y) direction, while the probe pulse, polarized at 45° with respect to the x axis, propagates along the y axis. All pulses are focused and intersect at a right angle on the molecular jet axis. The delay between P_1 and P_2 is set to half of the rotational period $T_r = 42.74$ ps of the CO_2 molecule. The data are recorded with a heterodyne detection [38].

Figure 2(a) shows the birefringence signal $\mathcal{S}_{xz} \propto n_x - n_z$ measured by tuning the probe delay τ over one rota-

tional period for an estimated peak intensity $I_2 \simeq 140$ TW/cm^2 and an intensity ratio $I_2/I_1 = 2.2$. The data recorded for $0 < \tau < T_r/2$ correspond to molecules exposed to a single pulse P_1. The latter being linearly polarized along the x direction, it is straightforward to show that $\mathcal{S}_{xz}$ is proportional to $\langle\cos^2\theta_x\rangle - 1/3$ [33]. The positive and negative transients feature hence molecules aligned along the field ($\langle\cos^2\theta_x\rangle > 1/3$, $n_x > n_z$) and delocalized in the (yz) plane perpendicular to the field ($\langle\cos^2\theta_x\rangle < 1/3$, $n_x < n_z$), respectively. The elevated baseline observed between the revivals reflects the permanent alignment induced along the field, whereas the negative signal produced at zero delay stems from the inversion of the electronic Kerr effect occurring at large intensity [39–41]. The second part of the trace, recorded for $\tau \geqslant T_r/2$, is related to the combined action of the cross-polarized pulses. The permanent alignment is enhanced by the second pulse P_2 as resulting from the delocalization of the molecules in the (xy) plane.

In order to assess the alignment achieved along the y axis, both horizontal polarizations depicted in Fig. 1 are rotated by 90°, so as from now on P_1 (resp., P_2) points along the y axis (resp., x axis). This is equivalent to having a probe beam propagating along the x axis, providing hence a signal given by $\mathcal{S}_{yz} \propto n_y - n_z$. The experimental result is presented in Fig. 2(b) for the same delay range and intensity ratio as in the previous measurement. For $\tau < T_r/2$, we see that the signal is not affected by the first pulse P_1 which is perpendicular to the probe wavefront. Conversely, for $\tau \geqslant T_r/2$, due to the anisotropy induced by P_2 on the wavefront of the probe, the signal exhibits the same features as in Fig. 2(a) but for $\tau < T_r/2$.

The value $\langle\cos^2\theta_z\rangle - 1/3$ reconstructed from $\mathcal{S}_{xz}$ and $\mathcal{S}_{yz}$ is shown in Fig. 2(c). More precisely, we plot the value $-\mathcal{S}_{xz} - \mathcal{S}_{yz} \propto \int \left[\langle\cos^2\theta_z\rangle - 1/3\right] \mathrm{d}V$ versus the delay, with $\int[\cdot]\mathrm{d}V$ denoting the integration over the interaction volume V (omitted in the previous discussion for simplicity's sake). First, we should notice that, for symmetry reasons, we have $\langle\cos^2\theta_z\rangle = \langle\cos^2\theta_y\rangle$ between the two aligning pulses, since P_1 vibrates along the x direction. This relation together with $\sum_l \langle\cos^2\theta_l\rangle = 1$ leads to $\langle\cos^2\theta_z\rangle - 1/3 = -\left(\langle\cos^2\theta_x\rangle - 1/3\right)/2$ during this time lag. The effect produced along the z and x axes are therefore out of phase for $\tau < T_r/2$, as attested by the comparison of Figs. 2(c) and (a), respectively. Secondly, the application of the second pulse P_2 results in a strong field-free delocalization of the molecules in the polarization plane of the bi-pulse for $\tau \geqslant T_r/2$, as predicted in Ref. [23]. In fact, we can see that the remaining transient components present a modulation which does not exceed the amplitude of the permanent one. This provides clear evidence that, even at moderately low temperature, the bi-pulse strategy allows to produce a significant planar alignment.

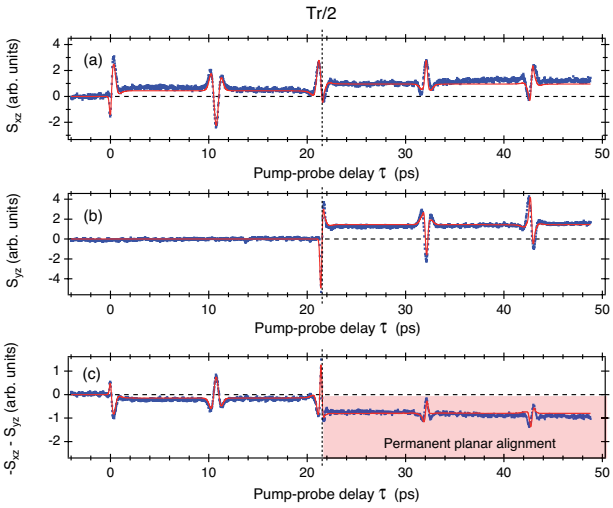

FIG. 2: (a) (Color online) Transient birefringence signal $\mathcal{S}_{xz} \propto n_x - n_z$ of CO_2 measured between the space-fixed x and z axes. (b) $\mathcal{S}_{yz} \propto n_y - n_z$. (c) $-\mathcal{S}_{xz} - \mathcal{S}_{yz}$ proportional to the space averaged value $\langle\cos^2\theta_z\rangle - 1/3$. The half of the rotational period of CO_2 is $T_r/2 = 21.37$ ps (vertical dashed lines). Experimental and calculated data are represented respectively by blue dots and red lines.

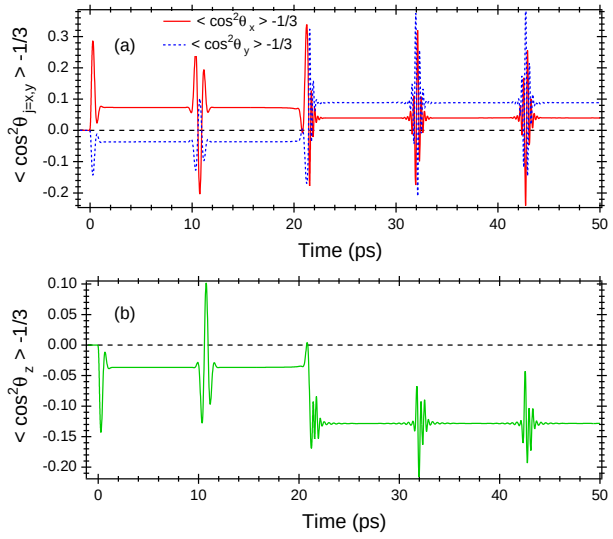

FIG. 3: (Color online) Evolution at $T = 100$ K of the expectation values (a) $\langle\cos^2\theta_x\rangle$ (red line), $\langle\cos^2\theta_y\rangle$ (dotted blue line), and (b) $\langle\cos^2\theta_z\rangle$ (green line) for the CO_2 molecule exposed to the peak intensities $I_y = 120$ TW/cm^2 and $I_x = I_y/2.2$.

B. Theory

In order to support the experimental findings, we numerically investigate the system under the present experimental conditions. For that purpose, we consider a linear molecule modelizing CO_2 in its ground vibronic

state which is subject to a non-resonant interaction with a laser field of the form

$$\vec{\mathcal{E}}(t) = E_x(t)\cos(\omega t)\vec{e}_x + E_y(t - T_{\rm r}/2)\cos(\omega t + \phi(t))\vec{e}_y, \quad (1)$$

where ω is the angular frequency and $\phi(t)$ the phase difference between the two polarization directions. We denote respectively by $E_x(t)$ and $E_y(t - T_{\rm r}/2)$ the temporal envelopes of the electric field along the x and y axes, $T_{\rm r}/2$ being the temporal delay between the two pulses. Within the rigid rotor approximation, the Hamiltonian of the system obtained after averaging over the rapid oscillations of the field can be written as

$$\begin{aligned} H(t) = \quad & BJ^2 - \frac{1}{4}[E_x^2(t)(\alpha_\perp + \Delta\alpha\cos^2\theta_x) \\ & + E_y^2(t - T_{\rm r}/2)(\alpha_\perp + \Delta\alpha\cos^2\theta_y)]. \end{aligned}$$

In the expression of the Hamiltonian, the first term represents the field-free rotational Hamiltonian, with the rotational constant B and the angular momentum operator J^2. For the numerical applications, we use for the CO_2 molecule the following parameters $B = 0.3902$ cm^{-1}, $\alpha_\parallel = 27.2984$ and $\alpha_\perp = 12.7908$ in atomic units. We consider for E_x and E_y gaussian envelopes written as $E_0 \exp[-t^2/\sigma^2]$, where E_0 is the maximum amplitude and $\sqrt{2\ln 2}\sigma$ is the pulse duration [full width at half maximum (FWHM)], which is assumed to be equal to 100 fs to simulate the experiments.

For a non-zero temperature, the system is described by a density operator $\rho(t)$ whose dynamics is governed by the von Neumann equation

$$i\frac{\partial\rho(t)}{\partial t} = [H(t), \rho(t)] \quad (2)$$

with the Boltzmann distribution at initial condition as

$$\frac{1}{Z}\sum_{j=0}^{\infty}\sum_{m=-j}^{j} |j,m\rangle e^{-Bj(j+1)/(k_{\rm B}T)}\langle j,m|, \quad (3)$$

where $Z = \sum_{j=0}^{\infty}\sum_{m=-j}^{j} e^{-Bj(j+1)/(k_{\rm B}T)}$ is the partition function, with $k_{\rm B}$ the Boltzmann constant, and $|j,m\rangle$'s the eigenvectors of J^2. In this formalism, the expectation value of any observable A is given by $\langle A\rangle(t) = {\rm Tr}[\rho(t)A]$.

We present the numerical results in Fig. 3 at $T = 100$ K and for the peak intensities $I_y \propto E_{0y}^2 = 120$ TW/cm^2 and $I_x = I_y/2.2$. Figure 3 displays the time evolution of the expectation values of the three director cosines during the interaction with the bi-pulse and over a field-free rotational period. In spite of a moderately low temperature, a substantial permanent planar alignment is achieved with a value of $\langle\cos^2\theta_z\rangle - 1/3 = -0.13$. Note also the symmetry of the dynamics of the two other expectation values $\langle\cos^2\theta_x\rangle$ and $\langle\cos^2\theta_y\rangle$ which is a signature of the planar alignment. This computation confirms the efficiency of the bi-pulse process which is not the optimal solution, but sufficiently simple to be experimentally implemented. A complete numerical study of the different strategies constructed from optimal control theory [42, 43] and evolutionary algorithm [17, 18] can be found in [23]. In particular, it can be shown that the ratio $I_y/I_x = 2.2$ is a good compromise for the bipulse strategy considering the laser intensity distribution and the temperature achieved in the experiment. The angular distribution computed at $t = T_{\rm r}/8$ after switch off of the second pulse (corresponding to $\tau = 26.71$ ps in Fig.2) is represented in Fig. 4. We recall that, when no field is applied, this distribution is spherical which means that any space direction is equivalent. When the molecule is aligned in a given direction, the probability distribution is peaked along the corresponding axis. In the case of planar alignment, the probability is delocalized in a plane as can be seen in Fig. 4. Note that the x and the y axes are not equivalent since the alignment along the y direction is better than along the x one, giving rise to a rectangular-like shape. This dissymmetry between the two axes can also be observed in Fig. 3 where the permanent values of $\langle\cos^2\theta_x\rangle$ and $\langle\cos^2\theta_y\rangle$ are clearly different. The qualitative discussion of Sec. II about the effect of the bipulse strategy on the population of the states $|J,M\rangle$ is quantitatively illustrated in Fig. 5. As could be expected, the two pulses, when successively applied, populate levels with higher and higher J and M quantum numbers. With respect to the initial Boltzmann distribution, the bipulse process leads however to a depletion of the population in the center of the diagram where $J \gg |M|$, and produces an increase of this population in the boundaries of the diagram where $J \simeq |M|$. This observation is in agreement with the fact that states with $J \simeq |M|$ maximize the planar alignment as shown in [23].

The numerical simulations described above are used to fit the experimental data presented in Fig. 2. Two free parameters have to be adjusted in order to compare the theoretical and the experimental results. The first one is a scaling factor and the second is the laser peak intensity. In order to account for the volume effects, the simulated signals are averaged over the spatial distributions of the laser beams. Doing so, a reasonable match between theory and experiment has been obtained in Fig. 2.

IV. CONCLUSION

We have presented an experimental demonstration of permanent planar alignment in a linear molecule. We have used a simple control strategy composed of two delayed short pulses linearly polarized in two orthogonal directions. This study calls for further investigations about the extensions of the concept of planar alignment. Having confined the molecular axis in a plane, the next step could be the control of the planar dynamics of the molecule by using a third laser pulse so as to control the sense of rotation of the molecular axis [22] or to transform the molecule in a quantum cogwheel [44].

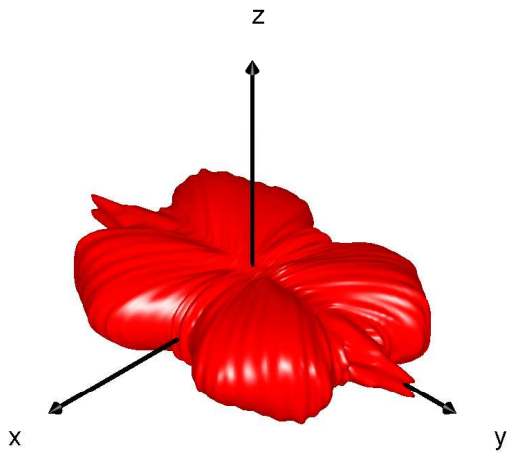

FIG. 4: (Color online) Angular distribution of the CO_2 molecule computed at $t = T_r/8$ after the interaction with the bi-pulse of intensities $I_y = 120$ TW/cm^2 and $I_x = I_y/2.2$. The temperature is $T = 100$ K.

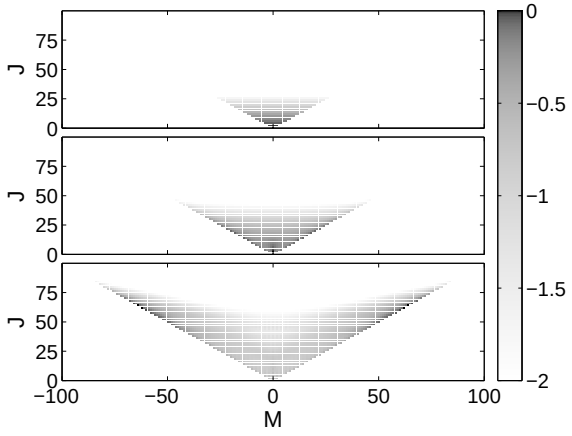

FIG. 5: Population distribution of the states $|J, M\rangle$ before the first pulse (top), between the two pulses (middle), and after the bi-pulse process (bottom). Same conditions as in Fig. 4. A grey scale has been used to represent the populations $a_{J,M}$ of the $|J, M\rangle$ states. The different gray levels correspond to $\log(a_{J,M}/\max_{J,M}[a_{J,M}])$. Note that in the CO_2 molecule, only the even J levels are populated.

Acknowledgments

We thank R. Saint-Loup, V. Tissot, B. Sinardet, S. Pernot, J.-M. Müller, and A. Javelle for valuable technical support. This work was supported by the Conseil Régional de Bourgogne, the ANR *COMOC*, and the *FASTQUAST* ITN Program of the 7th FP.

[1] J. Itatani, D. Zeidler, J. Levesque, M. Spanner, D. M. Villeneuve, and P. B. Corkum, Phys. Rev. Lett. **94**, 123902 (2005).
[2] S. Haessler, J. Caillat, W. Boutu, C. Giovanetti-Teixeira, T. Ruchon, T. Auguste, Z. Diveki, P. Breger, A. Maquet, B. Carré, et al., Nature Phys. **6**, 200 (2010).
[3] J. Itatani, J. Levesque, D. Zeidler, H. Niikura, H. Pépin, J. C. Kieffer, P. B. Corkum, and D. M. Villeneuve, Nature **432**, 867 (2004).
[4] M. Meckel, D. Comtois, D. Zeidler, A. Staudte, D. Pavičić, H. C. Bandulet, H. Pépin, J. C. Kieffer, R. Dörner, D. M. Villeneuve, et al., Science **320**, 1478 (2008).
[5] C. Z. Bisgaard, O. J. Clarkin, G. Wu, A. M. D. Lee, O. Geßner, C. C. Hayden, and A. Stolow, Science **323**, 1464 (2009).
[6] L. Holmegaard, J. L. Hansen, L. Kalhøj, S. L. Kragh, H. Stapelfeldt, F. Filsinger, J. Küpper, G. Meijer, D. Dimitrovski, M. Abu-samha, et al., Nature Phys. **6**, 428 (2010).

[7] J. L. Hansen, H. Stapelfeldt, D. Dimitrovski, M. Abusamha, C. P. J. Martiny, and L. B. Madsen, Phys. Rev. Lett. **106**, 073001 (2011).

[8] M. G. Reuter, M. Sukharev, and T. Seideman, Phys. Rev. Lett. **101**, 208303 (2008).

[9] F. Calegari, C. Vozzi, and S. Stagira, Phys. Rev. A **79**, 023827 (2009).

[10] J. Wu, P. Lu, J. Liu, H. Li, H. Pan, and H. Zeng, Appl. Phys. Lett. **97**, 161106 (2010).

[11] E. Hertz, B. Lavorel, and O. Faucher, Nature Photon. **5**, 89 (2011).

[12] A. G. York and H. M. Milchberg, Opt. Express **16**, 10557 (2008).

[13] J. Wu, Y. Tong, M. Li, H. Pan, and H. Zeng, Phys. Rev. A **82**, 053416 (2010).

[14] H. Stapelfeldt and T. Seideman, Rev. Mod. Phys. **75**, 543 (2003).

[15] V. Kumarappan, S. S. Viftrup, L. Holmegaard, C. Z. Bisgaard, and H. Stapelfeldt, Phys. Scr. **76**, C63 (2007).

[16] T. Seideman and E. Hamilton, Adv. At. Mol. Opt. Phys. **52**, 289 (2006).

[17] C. Horn, M. Wollenhaupt, M. Krug, T. Baumert, R. de Nalda, and L. Bañares, Phys. Rev. A **73**, 31401(R) (2006).

[18] E. Hertz, A. Rouzée, S. Guérin, B. Lavorel, and O. Faucher, Phys. Rev. A **75**, 031403(R) (2007).

[19] E. Gershnabel and I. S. Averbukh, Phys. Rev. Lett. **104**, 153001 (2010).

[20] K. Kitano, H. Hasegawa, and Y. Ohshima, Phys. Rev. Lett. **103**, 223002 (2009).

[21] A. G. York, Opt. Express **17**, 13671 (2009).

[22] Y. Khodorkovsky, K. Kitano, H. Hasegawa, Y. Ohshima, and I. S. Averbukh, Phys. Rev. A **83**, 023423 (2011).

[23] M. Lapert, E. Hertz, S. Guérin, and D. Sugny, Phys. Rev. A **80**, 051403 (2009).

[24] A. Gerbi, L. Vattuone, M. Rocca, U. Valbusa, F. Pirani, D. Cappelletti, and F. Vecchiocattivi, J. Chem. Phys. **123**, 224709 (2005).

[25] I. Nevo, S. Kapishnikov, A. Birman, M. Dong, S. R. Cohen, K. Kjaer, F. Besenbacher, H. Stapelfeldt, T. Seideman, and L. Leiserowitz, J. Chem. Phys. **130**, 144704 (2009).

[26] R. W. Boyd, *Nonlinear Optics* (Academic Press, Boston, 2008), 3rd ed.

[27] E. Gershnabel and I. S. Averbukh, Phys. Rev. A **82**, 033401 (2010).

[28] J. Floß, E. Gershnabel, and I. S. Averbukh, Phys. Rev. A **83**, 025401 (2011).

[29] O. Faucher, B. Lavorel, E. Hertz, and F. Chaussard (Springer, 2011), vol. VII of *Progress in Ultrafast Intense Laser Science VII*.

[30] V. Renard, O. Faucher, and B. Lavorel, Opt. Lett. **30**, 70 (2005).

[31] Y. Feng, H. Pan, J. Liu, C. Chen, J. Wu, and H. Zeng, Opt. Express **19**, 2852 (2011).

[32] V. Loriot, E. Hertz, B. Lavorel, and O. Faucher, J. Phys. B **41**, 015604 (2008).

[33] V. Renard, M. Renard, A. Rouzée, S. Guérin, H. R. Jauslin, B. Lavorel, and O. Faucher, Phys. Rev. A **70**, 033420 (2004).

[34] B. J. Sussman, J. G. Underwood, R. Lausten, M. Ivanov, and A. Stolow, Phys. Rev. A **73**, 53403 (2006).

[35] N. Xu, C. Wu, and Y. Gao, Appl. Phys. B **97**, 635 (2009).

[36] J. P. Cryan, P. H. Bucksbaum, and R. N. Coffee, Phys. Rev. A **80**, 063412 (2009).

[37] A. Rouzée, S. Guérin, O. Faucher, and B. Lavorel, Phys. Rev. A **77**, 043412 (2008).

[38] B. Lavorel, O. Faucher, M. Morgen, and R. Chaux, J. Raman Spectrosc. **31**, 77 (2000).

[39] V. Loriot, E. Hertz, O. Faucher, and B. Lavorel, Opt. Express **17**, 13429 (2009).

[40] V. Loriot, E. Hertz, O. Faucher, and B. Lavorel, Opt. Express **18**, 3011 (E) (2010).

[41] C. Brée, A. Demircan, and G. Steinmeyer, Phys. Rev. Lett. **106**, 183902 (2011).

[42] M. Lapert, R. Tehini, G. Turinici, and D. Sugny, Phys. Rev. A **78**, 023408 (2008).

[43] M. Lapert, R. Tehini, G. Turinici, and D. Sugny, Phys. Rev. A **79**, 063411 (2009).

[44] M. Lapert, S. Guérin, and D. Sugny, Phys. Rev. A **83**, 013403 (2011).